

Computational simulation of an IF-steel deformed by equal channel angular pressing via the finite element method

Neil de Medeiros, Shimeni Ribeiro Baptista,
Luciano Pessanha Moreira, Jefferson Fabrício Cardoso Lins and
Jayme Pereira de Gouvêa
*Universidade Federal Fluminense, Escola de Engenharia Industrial
Metalúrgica de Volta Redonda, Volta Redonda, RJ – Brazil*

Abstract

The objective of this work is to evaluate the equivalent plastic strain levels induced by equal channel angular pressing (ECAP) in an IF-steel billet after one pass at room temperature using the finite element method (FEM). For this purpose two-dimensional models were developed using a plane strain condition. It can be concluded that the simulation of this ultra-low carbon steels be interpreted as a quasi-static process because accurate results were observed in comparison to the analytical models reported in the literature.

Keywords: ECAP, severe plastic deformation, FEM, IF steel.

1 Introduction

The processing of nanostructured materials by mean of severe plastic deformation methods (SPD) has attracted a great scientific interest, mainly by the advantages of the SPD materials in comparison to other nanostructured materials [1]. Special metal forming methods were developed and used to this finality. One of the most prospective candidate for many practical applications is the equal channel angular pressing (ECAP) [2]. This method was invented by Segal [3,4] and is upon the of the simple shear strain-path in the optimization of some metal forming operations [5,6]. In this method a well lubricated billet is extruded by a plunger through a special die. Machined with two channels of constant cross-section, which intersect angle Φ is generally 90° . The principle of the ECAP method is schematically shown in Figure 1 [7]. In this figure, the angle Ψ defines the outer curvature of the intersection between the two channels.

The ECAP is a very interesting method provided that the billet has no significant shape changes and the accumulated plastic strains are very high in comparison to the traditional metal forming operations, such as the cold rolling and the drawing processes. Therefore, the comprehension of the

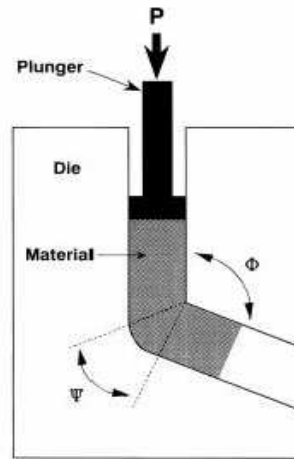


Figure 1: Schematic view of the equal channel angular pressing (ECAP) method [7].

mechanics of deformation occurring during the ECAP process is very important so as to evaluate the microstructure and the grain refinement attained as a

function of the deformations routes. In this context, the use of the extreme principles, for instance, the upper bound method has gained a lot of attention to estimate the pressure needed for the plunger as well as the accumulated effective strain resulting from the ECAP method [8–10]. In addition, the numerical simulation with the help of the finite element method (FEM) has been extensively used to better understating the ECAP method [11–16].

In the present work, a quasi-static solution to the ECAP method by the FEM simulation was carried out using dies with intersecting angles $\Phi = 90^\circ$ and 120° , considering only one pass of extrusion and adopting a plane strain state. A frictionless condition was used to compare the effective strain and extrusion force obtained by FEM and those predicted by upper bound solution. In addition, values of 0.05 and 0.1 to the friction coefficient were adopted to study the development of the uniform plastic strain zone. In all cases, the generalized Coulomb law was assumed.

2 Analytical solutions of the effective plastic strain and extrusion pressure

Iwahashi and et al. (works) [8] have proposed, in 1996, a relation between effective strain, ε_{eff} , and the ECAP angles Φ and Ψ . This expression is calculated from von Mises isotropic yield criterion applied to the pure shear condition as:

$$\varepsilon_{eff} = \frac{N}{\sqrt{3}} \left[2 \cot \left(\frac{\Phi}{2} + \frac{\Psi}{2} \right) + \Psi \operatorname{cosec} \left(\frac{\Phi}{2} + \frac{\Psi}{2} \right) \right] \quad (1)$$

where N the number of the extrusion passes. Here, to $N = 1$ and $\Psi = 0^\circ$, equation (1) reduces in the previously relation obtained by Segal [6]:

$$\varepsilon_{eff} = \frac{2}{\sqrt{3}} \left[\cot \left(\frac{\Phi}{2} \right) \right] \quad (2)$$

Alkorta *et al.* [9] proposed an upper bound solution to the ECAP pressure considering Hollomon-type materials and using a frictionless condition. According to these authors, the pressure is related with the material hardening behavior as follows:

$$P_{ECAP} = \left(\frac{\sigma_0}{n+1} \right) \left[\frac{2 \cot \left(\frac{\Phi+\Psi}{2} \right) + \Psi}{\sqrt{3}} \right]^{(n+1)} \quad (3)$$

where σ_0 and n are the yield stress and the strain-hardening exponent, respectively.

Based in this study, an analogue ECAP pressure solution considering a Swift-type material is adopted in the present work, $\bar{\sigma} = K(\varepsilon_0 + \bar{\varepsilon}^p)^n$, where K is the strength coefficient, ε_0 is the pre-strain and $\bar{\varepsilon}^p$ is effective von Mises plastic strain. Thus, considering one pass of extrusion, the equation (3) becomes:

$$P_{ECAP} = \left(\frac{K}{n+1} \right) \left\{ \left[\left(\frac{\sigma_0}{K} \right)^{\left(\frac{1}{n} \right)} + \left(\frac{2 \cot \left(\frac{\Phi+\Psi}{2} \right) + \Psi}{\sqrt{3}} \right) \right]^{(n+1)} - \left[\left(\frac{\sigma_0}{K} \right)^{\left(\frac{1}{n} \right)} \right]^{(n+1)} \right\} \quad (4)$$

The extrusion force per unit of thickness, after one pass, can be obtained multiplying the right side of the equation (4) by the width (W) of the billet. Thus,

$$\frac{F_{ECAP}}{thickness} = W \left(\frac{K}{n+1} \right) \left\{ \left[\left(\frac{\sigma_0}{K} \right)^{\left(\frac{1}{n} \right)} + \left(\frac{2 \cot \left(\frac{\Phi+\Psi}{2} \right) + \Psi}{\sqrt{3}} \right) \right]^{(n+1)} - \left[\left(\frac{\sigma_0}{K} \right)^{\left(\frac{1}{n} \right)} \right]^{(n+1)} \right\} \quad (5)$$

The F_{ECAP} calculations were carried out through a computational code developed in Fortran language. A billet of 50 mm (height) x 10 mm (width) and unitary thickness is considered. The material analyzed in this work is an IF steel which is described in uniaxial tension by $K= 544.96$ MPa, $\varepsilon_0=0.004852$ and $N= 0.235$, according to reference [17].

3 The finite element analysis

The simulation of the extrusion of the IF steel billet was made by assuming isothermal conditions at room temperature and neglecting the heating conditions due to the friction between the workpiece and the die tool. The numerical simulations were performed with commercial finite element code ANSYS. The details of the FEM modeling are described as follows.

3.1 Modeling of the die

Two distinct models for the ECAP die were developed. One considering the channels intersection angle $\Phi = 90^\circ$ and another $\Phi = 120^\circ$. In both cases, the angle Ψ was assumed to be zero. The dies were assumed to be rigid pieces and the material used was an H13 tool-steel with the Young modulus E and the Poisson's ratio ν equal to 200,000 MPa and 0.3 respectively.

The details of the channels are shown in Figure 2. It can be noted the presence of a curvature radius of 1.5 mm at the top channels intersection. It was necessary to the convergence of the solution, according to Luis-Pérez [18]. The choice of this particular die geometry is in agreement with the ECAP design in progress in the Laboratory of Mechanical Tests at the Federal Fluminense University (EEIMVR/UFF).

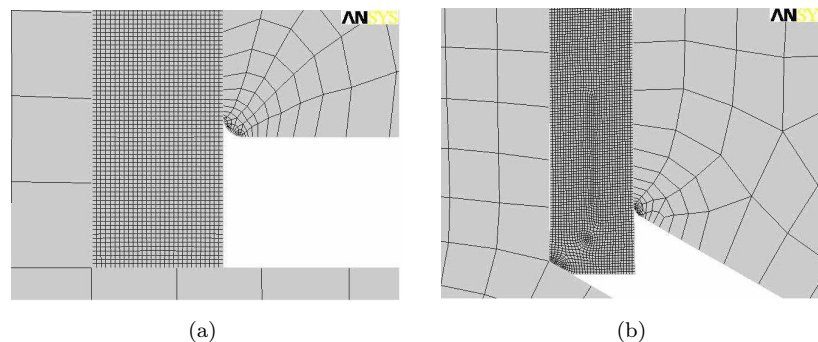


Figure 2: Details of the two-dimensional ECAP die tooling FEM modeling: (a) intersection angle $\Phi = 90^\circ$ and (b) intersection angle $\Phi = 120^\circ$.

3.2 Modeling of the billet

The two-dimensional workpiece considered has the dimensions of 10 mm (width) x 50 mm (height) and a unity thickness since a plane-strain condition is assumed.

The material of the billet was assumed to be isotropic elastic-plastic and its elastic properties were $E = 195,000$ MPa and $\nu = 0.29$ whereas the plasticity is defined by the von Mises or J2 associated flow rule. The billet is described by 4,590 linear four-node plane-strain elements, PLANE 182 according to the ANSYS terminology [19].

3.3 Loadings and workpiece-tooling contact

The plunger is not taking into account the finite element modeling. It has been replaced by a displacement boundary condition imposed to the top nodes of the billet as shown in Figure 3. In order to assure the quadratic convergence of the Newton-Raphson method used in the ANSYS code, the top billet displacements were fixed in increments of 0.25 mm up to a total displacement of 45 mm.

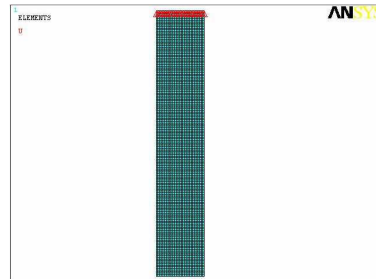


Figure 3: Boundary displacements applied on the top nodes of the billet, represented by the red symbols.

Concerning the friction behavior at the workpiece-tooling interface, the friction coefficient values of 0, 0.05 and 0.1 were attributed at the models to carried out the simulations. To represent the friction behavior, the generalized Coulomb's law was used in the FEM models.

How known, the generalized Coulomb's law states a relation between yield stresses in pure shear and uniaxial tension, respectively. Specifically in the Ansys program, this relation is verified by mean of von Mises yield criterion corrected to pure shear condition and is given by:

$$\tau_{MAX} = \frac{\sigma_Y}{\sqrt{3}} \quad (6)$$

where τ_{MAX} and σ_Y are the yield stresses in pure shear and uniaxial tension, respectively. Thus, to stress values lesser than τ_{MAX} , sliding of the workpiece is observed and to higher or equal values of τ_{MAX} , an adherence condition has occurred, like a weld.

Finally, a flexible contact between workpiece and tool was employed. For this step, CONTA 171 [18] and TARGE 169 [18] elements have been used. The contact regions assumed were in relation of the billet, it left, right and bottom sides and to the dies the contact regions were the channel lines next to the billet. Figure 4 shows these contact regions. There, only bottom portions of the models are shown and the coarse black and blue lines represent the contact considered to each die configuration. The contact status was updated after each load step to avoid inaccurate results. Thus, taking in account the die geometries considered, the total time spent in the simulations does not exceed 6 hours, using a Pentium IV computer with 4GB of RAM memory.

4 Results and discussions

4.1 Extrusion force and effective strain obtained by the upper bound method and FEM: frictionless condition

In the absence of the friction, the extrusion force per unit of thickness obtained from equation (5) is greater than FEM simulations in both $\Phi = 90$ and 120° , as shown in Figure 5(a). Besides,

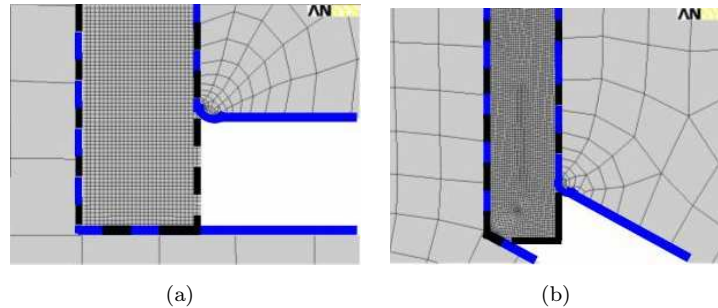


Figure 4: Details of the contact workpiece-tool; (a) contact regions to 90° die; (b) contact regions to 120° die. The black coarse traced lines refer to billet contact and blue coarse traced lines refer to die contact regions.

the force increases with decreasing Φ angles as reported in the literature [9, 10, 18, 20]. The FEM results presented in Figure 5(a) represent an average value obtained from regions AB ($\Phi = 90^\circ$) and CD ($\Phi = 120^\circ$), where the ECAP force has reached a steady-state condition, see Figure 5(b). The distinct behavior of these curves can be explained by the fact of the normal pressure at 90° is greater than at 120° due to the bending- unbending effect, which is more important in the first case.

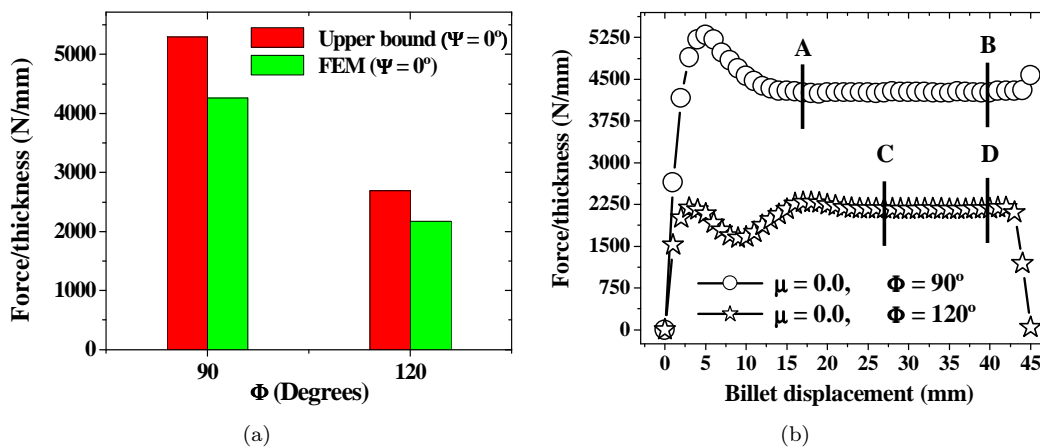


Figure 5: (a) comparison between upper bound and FEM extrusion forces; (b) extrusion force vs. displacement on the billet, illustrating the regions of average values used in (a).

A decrease of the Φ angle is directly linked to the attainment of higher effective plastic strains. This

is confirmed in Figure 6 wherein the FEM values were calculated by averaging the nodal results in the path traced along the homogeneous strain zone, obtained after 45 mm of the billet displacement. The paths used in both die configurations to obtain the effective plastic strains are represented in Figure 7 by black arrows where its limits are delimited by nodes I and J depicted by black dots.

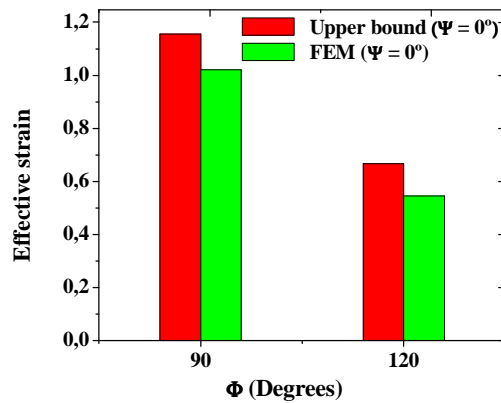


Figure 6: Comparison between the upper bound and FEM predictions of the effective plastic strains obtained for $\Phi = 90$ and 120 degrees.

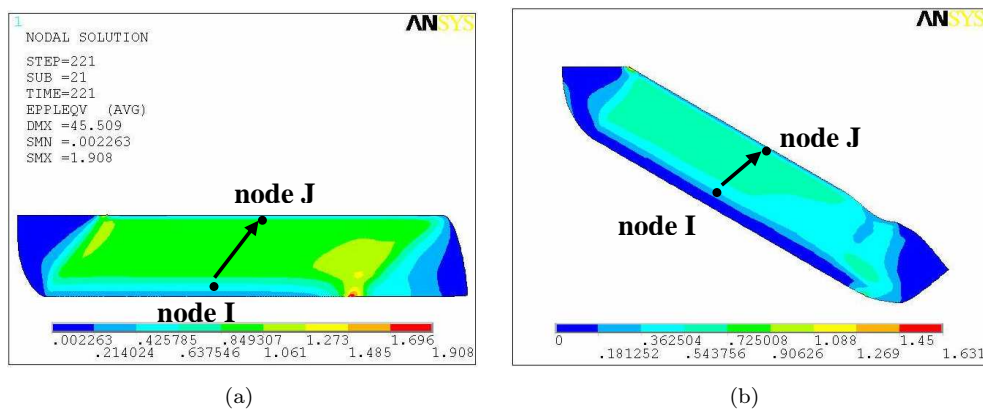


Figure 7: Procedure to obtain the average values for the effective plastic strains: (a) $\Phi = 90^\circ$; (b) $\Phi = 120^\circ$.

4.2 Friction stresses and effective plastic strains as a function of the μ -value

The appearance of a shear plane at 45° between the two channels is independent of the friction condition as well as of the intersection angle Φ . Figure 8 presents the numerical predictions for the friction stress and the contact pressure as a function of the μ -value obtained for $\Phi = 90^\circ$ from the nodes located at the left and right billet sides. It is worth to note an inversion of the friction stresses sign which is attributed to the passage of the billet towards the second channel. Also, either the friction stress or the contact pressure increases with the friction coefficient and, in particular, higher μ -values provide a sticking friction condition as observed at the billet right side for displacement $U_y = 20$ mm. This explains the outlet inwards rounded shape of the billet, as shown in Figure 7(a).

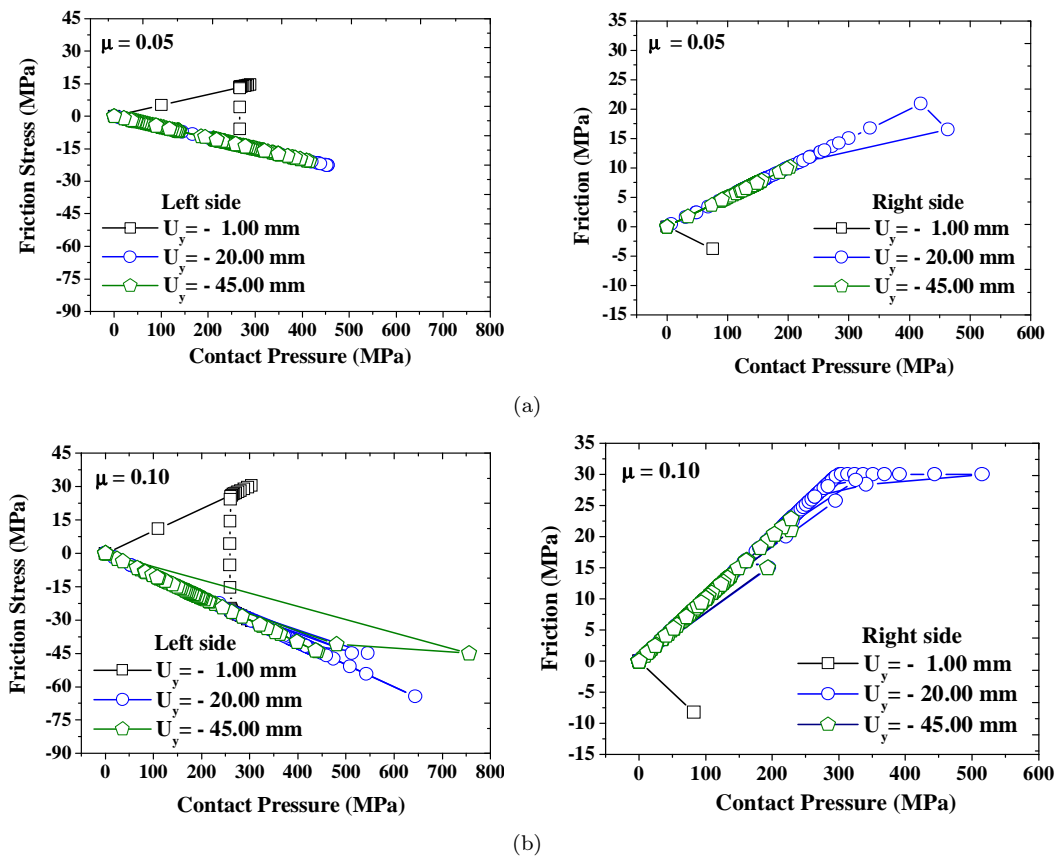


Figure 8: Friction stress and die contact pressure obtained for $\Phi = 90^\circ$ from the nodal values located at the left and billet right sides: (a) $\mu = 0.05$ and (b) $\mu = 0.10$.

On the other hand, Figure 9 compares the reaction nodal forces determined for $\Phi = 90^\circ$ and 120° as a function of the μ -value and the billet displacement. As expected, the increasing in the friction coefficient requires higher extrusion pressures or punch loads. Also, it can be observed an increase of the reaction forces up to about 7.5 mm and 5 mm for the intersecting angles $\Phi = 90^\circ$ and $\Phi = 120^\circ$ respectively followed by a decreasing up to about 10 mm, which corresponds to the channels width, which is due to the first bending of the billet edge. For $\Phi = 90^\circ$, a common initial behavior is observed for all the extrusion forces with a peak, due to the inwards rounded shape of the billet as shown in Figure 10(a), followed by an immediate unloading caused by the inversion of the shear stresses sign. Next, a progressive and approximately linear increasing of the nodal extrusion force is noted when $\mu = 0.05$ whereas there is a drop for $\mu = 0.10$ due to the adherence of the billet right side at the second channel. Conversely, the force evolution obtained for $\Phi = 120^\circ$ shows a reloading up to 15 mm due to the second bending needed to complete the rotation of the billet, see Figure 10 (b).

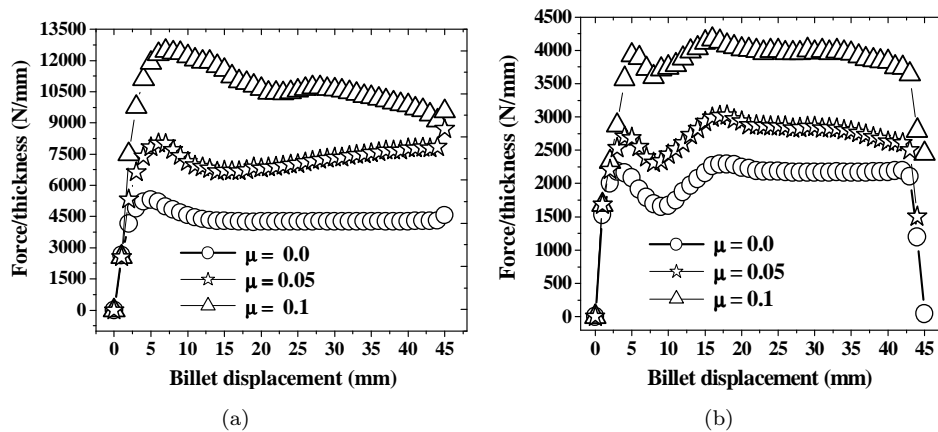


Figure 9: Extrusion forces in function of the friction conditions: (a) $\Phi = 90^\circ$; (b) $\Phi = 120^\circ$.

Figure 11 shows the iso-contours plots of the effective von Mises plastic strains and stresses determined for $\Phi = 90$ and $\mu = 0.05$. Firstly, one can observe that either the bottom or the top of the billet present the smallest effective strains since these regions do not pass through the 45° shear zone between the two channels. Secondly, the extremely high value of the effective plastic strain close to 2.4 is due to $\Psi = 0$ which leads to the mesh folding. Finally, the uniform regions of the effective plastic strains are originated by the stress flow lines normal to the direction of the displacements application, as previously reported by Kim *et al.* [11]. Besides, it can be important to note that the hardening curve obtained in uniaxial tests have a great limitation in the case of SPD simulations (where the $\varepsilon_{eff} > 1$), since the maximum von Mises plastic stress value observed in Figure 11(b) corresponds to the ultimate tensile of the curve. Thus, more representative results are provided by the use of a hardening curve from simple shear tests, for example torsion tests. Taking into account the plastic

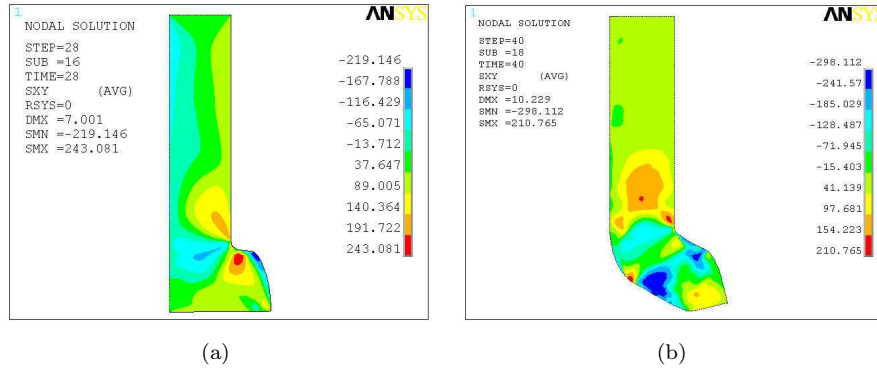


Figure 10: Shear stress distributions obtained for $\mu = 0.10$: (a) $\Phi = 90^\circ$ at $U_y = 7$ mm and (b) $\Phi = 120^\circ$ at $U_y = 10$ mm.

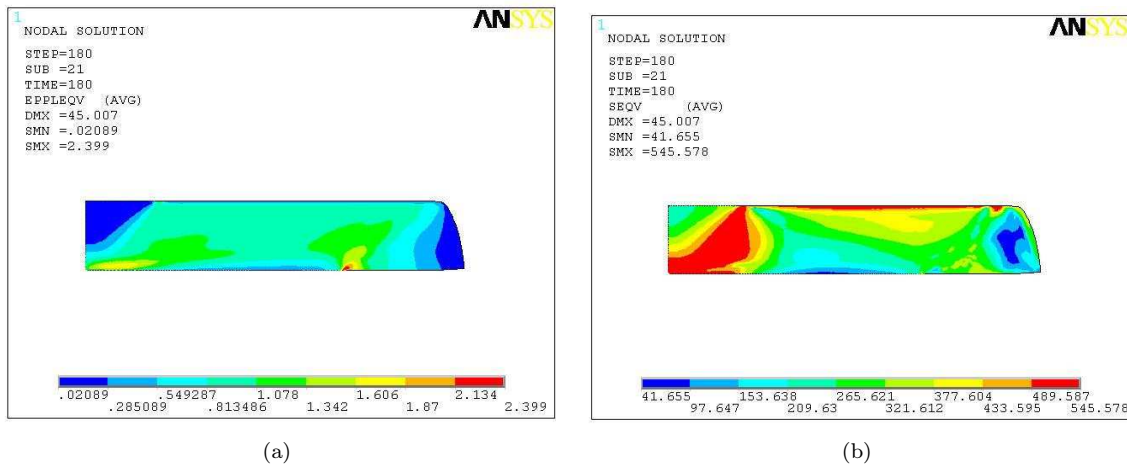


Figure 11: (a) Effective plastic strains to ($\mu = 0.05$) after 45 mm of displacement; (b) correspondent von Mises plastic stresses.

work equivalence, a correspondent uniaxial stress-strain curve is determined so and it possibilities the representation of the material behavior when very greats accumulated effective plastic strain are achieving, at each pass of ECAP extrusion.

5 Conclusions

The quasi-static FEM simulation of the one pass of the ECAP extrusion in an IF steel billet makes possible some conclusive observations, as follows:

1) The analytical upper bound solution for a Swift-type material also provided higher pressure (force/thickness) and effective plastic strains values being permitted to validate this approach and to suggest that a pre-deformation in the hardening material behavior before the ECAP method is a good alternative to analyze the workpiece plastic performance.

2) The existence of a shear plane at 45° in both 90° and 120° occurs independently of the friction condition and it is a direct consequence of the contact pressure on the outer region of the die. Moreover, the friction conditions have a great influence on the extrusion forces and effective strain, mainly at the $\Phi = 90^\circ$. At 120° , the friction influence on the effective strain was lesser than 90° showing a good agreement with the literature.

3) The adopting of the true hardening curve obtained from uniaxial tests permits an accurate analysis of the ECAP extrusion influence after one pass on the ductile materials, like IF steel. Moreover, to analyze the effective strains induced in two or more passes, the corrected procedure is to employ a true hardening curve obtained in a simple shear test, which represents in a correct form the plane strain condition commonly attributed in ECAP finite element models. Depending on the software used to carry out the simulation, like Ansys, the von Mises yielding criterion is used to consider plasticity. So, through the plastic work equivalence, a simple shear true hardening curve will be transformed into an uniaxial one, making possible the numerical simulation.

Acknowledgements

The authors wish to thank to research scholarship from CAPES.

References

- [1] Valiev, R. & Langdon, T., Principles of equal-channel angular pressing as a processing tool for grain refinement. *Progress in Materials Science*, **51**, pp. 881–981, 2006.
- [2] Segal, V., Engineering and commercialization of equal channel angular extrusion (ECAE). *A Materials Science and Engineering*, **386(269-279)**, 2004.
- [3] Valiev, R., Islamgaliev, R. & Alexandrov, I., Bulk nanostructured materials from severe plastic deformation. *Progress in Materials Science*, **45**, pp. 103–189, 2000.
- [4] Segal, V., *Methods of stress-strain analysis in metal-forming*. Ph.D. thesis, Minsk, 1974. (in English).
- [5] Segal, V., Reznikov, V., Drobyshchik, A. & V., K., Plastic working of metals by simple shear. *Russian Metallurgy*, **1**, pp. 99–105, 1981.
- [6] Segal, V., Materials processing by simple shear. *A Materials Science and Engineering*, **197**, pp. 157–164, 1995.
- [7] Nakashima, K., Horita, Z., T., M.N. & Langdon, Influence of channel angle on the development of ultrafine grains in equal-channel angular pressing. *Acta Materialia*, **46**, pp. 1589–1599, 1998.

- [8] Iwahashi, Y., Wang, W., Nemoto, M. & Langdon, T., Principle of equal-channel angular pressing for the processing of ultra-fine grained materials. *Scripta Materialia*, **35**, pp. 143–146, 1996.
- [9] Alkorta, J. & Sevillano, J., A comparison of fem and upper-bound type analysis of equal-channel angular pressing (ecap). *Journal of Materials Processing Technology*, **141**, pp. 313–318, 2003.
- [10] Luis-Pérez, C., Upper bound analysis and fem simulation of equal fillet radii angular pressing. *Modelling and Simulation in Materials Science and Engineering*, **12**, pp. 205–214, 2004.
- [11] Kim, H., Seo, M. & Hong, S., On the die corner gap formation in equal channel angular pressing. *A Materials Science and Engineering*, **291**, pp. 86–90, 2000.
- [12] Kim, H., Finite element analysis of equal channel angular pressing using a round corner die. *A Materials Science and Engineering*, **315**, pp. 122–128, 2001.
- [13] Oh, S. & Kang, S., Analysis of the billet deformation during equal channel angular pressing. *A Materials Science and Engineering*, **343**, pp. 107–115, 2003.
- [14] Nagasekhar, A. & Tick-Hon, Y., Optimal tool angles for equal channel angular extrusion of strain hardening materials by finite element analysis. *Computational Materials Science*, **30**, pp. 489–495, 2004.
- [15] Zhao, W., Ding, H., Ren, Y., Wang, J. & Wang, J., Finite element simulation of deformation behavior of pure aluminum during equal channel angular pressing. *A Materials Science and Engineering*, **410-411**, pp. 348–352, 2005.
- [16] Yoon, S., Seo, M. & Kim, H., Preform effect on the plastic deformation behavior of workpieces in equal channel angular pressing. *Scripta Materialia*, **55**, pp. 159–162, 2006.
- [17] Moreira, L., ao, E.R., Viana, C., Vieira, L. & Sampaio, A., Avaliação da anisotropia plástica de chapas finas através de ensaios automáticos de tração uniaxial. *4^o Seminário de Laminação: Processos e Produtos Laminados e Revestidos, Associação Brasileira de Metalurgia e Materiais*, Santos-SP - Brazil, volume 1, pp. 42–50, 2005. (in Portuguese).
- [18] Luis-Pérez, C., On the correct selection of the channel die in ecap processes. *Scripta Materialia*, **50**, pp. 387–393, 2004.
- [19] Swanson Analysis Systems Inc., *Ansys User's Manual for Revision 5.0*, 1994.
- [20] Eivani, A. & Taheri, A., An upper bound solution of ecae process with outer curved corner. *Journal of Materials Processing Technology*, **182(555-563)**.